Manhole Localization and Condition Diagnostics in Telecom Networks Using Distributed Acoustic and Temperature Sensing

Shaobo Han, Ming-Fang Huang, Yaowen Li, Glenn A. Wellbrock, Tiejun J. Xia, Scott Kotria, Jeffrey A. Mundt, James M. Moore, Philip Ji, Tingfeng Li, Yuheng Chen, Ting Wang and Yoshiaki Aono

(Top-Scored Paper)

***Abstract*—We present methods and field trial results demonstrating an integrated distributed acoustic sensing (DAS) and distributed temperature sensing (DTS) system for manhole localization, condition diagnostics, and anomaly detection in predeployed telecommunication fiber networks. The proposed system leverages ambient environmental signals, such as vibrational patterns from traffic and day-night temperature fluctuations, and machine learning techniques for automated detection. By combining DAS waterfall traces with temperature measurements from DTS, we achieve improved classification accuracy. Experimental results from three real-world testbeds in Texas and New Jersey show a significant improvement in classification accuracy—from 78.9% and 89.5% using DAS and DTS alone, respectively, to 94.7% via cross-referenced analysis. We propose a structured prediction formulation for manhole localization based on a U-Net architecture with a gated attention mechanism, where the label of each fiber location in the waterfall image is predicted using both its neighboring context and within-patch discriminative features. The method also supports cross-route generalization for manhole localization and enables condition diagnostics, identifying issues such as cable exposure and water ingress. These results highlight the potential for scalable deployment of fiber sensing solutions for real-time, continuous monitoring of telecom infrastructure.**

***Index Terms*—Deep learning, distributed acoustic sensing, distributed temperature sensing, infrastructure monitoring, localization, machine learning, sensor fusion.**

I. Introduction

Optical fiber cables, originally designed for telecommunications, are increasingly being repurposed for ambient environmental monitoring through fiber sensing technologies [1]–[4]. When a sensing pulse is launched into the fiber, light is scattered omnidirectionally at each position due to Rayleigh, Brillouin, and Raman backscattering. Rayleigh backscatter, which results from the inhomogeneities in the glass and retains the same frequency as the launched signal, is employed in Distributed Acoustic Sensing (DAS) based on phase-sensitive optical time domain reflectometry (ϕ-OTDR) for various applications, including traffic monitoring [5] and incident detection [6], cable damage detection [7], underwater sound surveillance [8], seismic monitoring [9], and perimeter intrusion detection [10]. Raman scattering involves nonlinear processes where the Stokes and anti-Stokes signals return at frequencies around ±13 THz from the launched signal. This phenomenon is utilized in Distributed Temperature Sensing (DTS) for applications such as pipeline leakage detection [11] and fire detection [12].

While DAS and DTS are traditionally used independently, integrating both sensing modalities provides complementary information that enhances monitoring reliability. DAS offers high temporal resolution and sensitivity to acoustic or vibration events, enabling detection of dynamic activities such as vehicle movement, or nearby construction. In contrast, DTS provides accurate, long-term temperature profiling along the same fiber, allowing detection of environmental changes such as flooding or abnormal heating. By combining these two sensing mechanisms, the system can correlate dynamic and static signals to improve event interpretation and reduce false alarms. Similar DAS/DTS integrations have shown proven benefits in other fields, such as oil and gas well monitoring [13], power cable diagnostics [14], and pipeline integrity management [15], where joint acoustic–thermal analysis enables more robust fault detection and localization. Motivated by these advantages, this work explores the joint use of DAS and DTS for reliable localization and condition monitoring of underground fiber cables deployed in manholes.

Recent advances in machine learning (ML) and artificial intelligence (AI) technologies have created exciting opportunities to bridge the gap between distributed fiber-optic sensing and real-world applications in noisy and complex deployment environments. Readers are referred to recent surveys [16], [17] for comprehensive overviews of this emerging research area. There is a growing body of research exploring cutting-edge ML techniques to enhance the performance of fiber-optic sensors. Examples include weakly supervised learning for signal denoising [18], conditional diffusion models for data imputation [19], and recurrent autoencoders for seismic data compression [20]. In addition, convolutional neural

Preprint version. (Corresponding author: Shaobo Han.)

Shaobo Han, Ming-Fang Huang, Yaowen Li, Philip Ji, Tingfeng Li, Yuheng Chen, and Ting Wang are with the NEC Laboratories America, Princeton, NJ 08540 USA (e-mail: shaobo@nec-labs.com; mhuang@nec-labs.com; yali@nec-labs.com; pji@nec-labs.com; tli@nec-labs.com; yuhengchen@nec-labs.com; ting@nec-labs.com).

Glenn A. Wellbrock, Tiejun J. Xia, Scott Kotria, and Jeffrey A. Mundt are with the Verizon, Richardson, TX 75081 USA (e-mail: glenn.wellbrock@verizon.com; tj.xia@verizon.com; scott.kotrla@verizon.com; jeff.mundt@verizon.com).

James M. Moore is with the Verizon, 999 W Main St, 02 Floor, Freehold, NJ 07728, USA (e-mail: james.m.moore@verizon.com).

Yoshiaki Aono is with the NEC Corporation, Abiko 270-1174, Japan (e-mail: jwa32@nec.com).

networks (ConvNets) have been proposed for marine animal sound classification [21]. Recent studies have also investigated the impact of data representation (e.g., short-time Fourier transform (STFT) spectrograms versus mel-frequency cepstral coefficients (MFCCs)) and model architecture (e.g., ConvNets versus vision transformers) on acoustic event recognition in telecom networks [10], as well as approaches to improve data efficiency through few-shot adaptation from pre-trained foundation models [22] and semi-supervised learning via energy-based generative models [23].

In modern telecom infrastructure—forming the backbone of 5G and future networks—a large proportion of fiber-optic cables is buried underground, with slack fiber segments typically stored in manholes (or handholes) along the route. It is essential for carriers and operators to accurately locate these manholes for maintenance purposes [24]. However, due to ongoing changes in fiber cables, such as branching, additional connections, and the incorporation of extra fibers, relying solely on the database and optical time-domain reflectometry (OTDR) may result in inaccurate manhole localization. OTDR lacks precision in pinpointing the actual geographic location. This limitation arises because the measured optical distance does not account for slack loops or routing variations along the fiber path, making it difficult for field technicians to locate the fault accurately on the ground.

To localize landmarks or key points along fiber routes, methods based on fiber sensing and machine learning techonologies have been proposed for automated localization by utilizing external vibrations, such as hammer strikes on manhole lids [25] and hammer knocks on utility poles [26]. However, these active excitation approaches require on-site visits and the deliberate generation of excitation signals, making them labor-intensive, time-consuming, and impractical for large-scale deployment.

To overcome this limitation, passive ambient vibration methods have been explored with automated manhole localization algorithms over existing telecom networks. In [27], an image patch classification–based approach is proposed that leverages ambient environmental data—such as traffic-induced vibrations—for manhole localization, thereby eliminating the need for manual excitation. Although environmental excitations can generate discriminative features, not all waterfall patches from manhole locations consistently exhibit them. As a result, the problem is considered *weakly supervised* since labels (manhole vs. non-manhole) are available only at the location level, not for every time period. Accordingly, a top-K data selection scheme [27] is proposed to enhance the witness rate (WR), which is the proportion of informative, manhole-indicative patterns within a manhole location.

In this paper, which is an extension to [28], we propose the design of an integrated DAS/DTS sensing system for localizing underground cable access points (manholes, hand holes, etc.), diagnosing their conditions, and detecting cable exposure anomalies, with field validation. We also introduce a structured prediction formulation for manhole localization based on a U-Net architecture [29] with attention gates [30] applied to spatial–temporal waterfall data. Our approach leverages a lightweight U-Net Attention model to perform dense spatial predictions along the fiber, thereby enabling high-accuracy localization. The proposed structured prediction formulation and U-Net Attention model are broadly applicable to a wide range of linear infrastructure monitoring applications, including railways, tunnels, pipelines, riverbanks, power transmission lines, and telecommunication cables.

The remainder of this paper is organized as follows. Section II presents the field trial setup and the integrated DAS/DTS system configuration. Section III describes the physical phenomena related to manhole localization and condition diagnosis. Section IV presents the proposed method. Section V provides experimental results from the field trials, including manhole localization based on cross-referencing DAS and DTS, condition diagnostics, and anomaly detection. Finally, Section VI concludes the paper.

II. Field Trial Experimental Setup

Figure 1(a) displays the experimental setup of integrated real-time DAS/DTS system. A 1550-nm laser diode (LD)was split by a $50:50$ coupler, where one branch is used as the local oscillator (LO) for the coherent receiver, and another branch passes through an acousto-optic modulator (AOM), erbium-doped fiber amplifier (EDFA) and dense wavelength division multiplexing (DWDM) filter, generates 40-ns sensing pulses, corresponding to a theoretical spatial resolution of approximately 4 meters along the sensing fiber. The system operates at a 2000 Hz repetition rate and a 125 MHz sampling rate, and through digital signal processing, interpolation, downsampling, and fast on-chip processing to achieve a spatial sampling interval as fine as 1.6 meter within the sensing coverage of 10 dB loss (approximately 50 km of standard single-mode fiber (SSMF) with 0.2 dB/km attenuation). Both Rayleigh and Raman backscattering signals are returned from the field and separated by DTS Raman filters. Further details of DAS/DTS system design can be found in [31].

The Rayleigh backscatters at 1550 nm are captured by an integrated coherent receiver (ICR), processed through digital signal processing (DSP) for the DAS function, while high-gain avalanche photodiodes (APDs) receive Raman backscatters at 1450 nm and 1660 nm, feeding into DSP for DTS functionality. By adjusting the peak power of the sensing probe, the system can selectively activate DAS at low peak power ($<$ 100 mW) and DTS at high peak power ($>$ 1 W). The DTS system provides a temperature resolution of approximately $\pm 1^{\circ}\mathrm{C}$ within the first 5 km and $\pm 2^{\circ}\mathrm{C}$ at end of 20 km, which is sufficient to resolve the environmental temperature fluctuations observed in this study. These environmental fluctuations typically range from several to more than ten degrees Celsius between day and night, confirming that the measured variations represent genuine thermal changes rather than measurement noise.

During field experiments, the two sensing modes were not operated concurrently. Instead, the system alternated between modes, approximately 1 minute for DTS measurements and 5 minutes for DAS measurements, allowing both acoustic and thermal responses to be characterized on the same fiber without hardware reconfiguration.

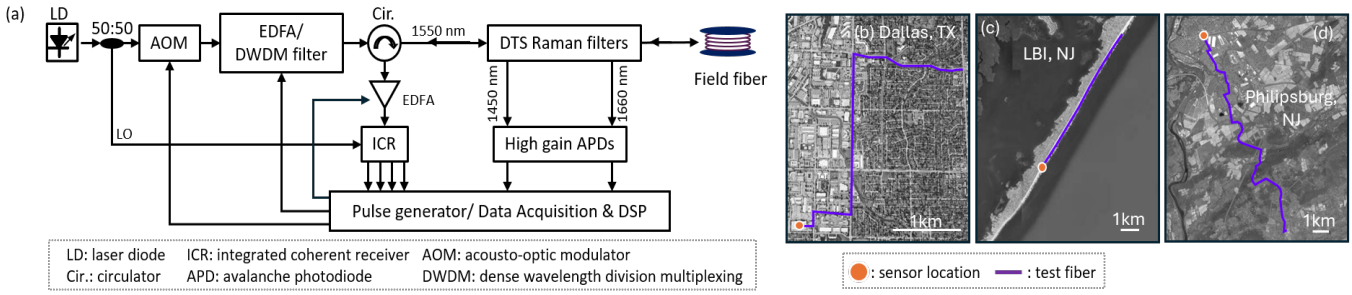

Fig. 1. (a) Experimental Setup (LO: local oscillator.). Testbeds in (b) Richardson, TX, (c) Long Beach Island and (d) Philipsburg, NJ.

Figure 1(b) and Figure 1(c) show the test beds in Richardson, TX, and Long Beach Island (LBI), NJ. The fiber length in Richardson test bed is approximately 5.8 km, while the LBI test bed covers about 5.2 km. Most cables are buried at depths of 36-48 inches (0.9−1.2 m) in TX and 40-60 inches (1−1.5 m) in NJ. These locations represent two different environmental conditions: the manhole in Richardson is typically dry, whereas those in LBI are often flooded. In this study, we employed two approaches: one that analyzes the temperature variations (ΔT) from DTS data, and a machine learning (ML)-based approach that processes DAS signals based on characteristic vibration patterns generated by passing traffic.

To capture temperature variations, data was analyzed during the warmest part of the day (∼2 pm) and the coolest part of the night (∼2 am). These windows represent peak thermal fluctuations, providing essential data for analysis. In this context, dry manhole and aerial cable sections with fiber lengths will be identified, while buried cables remain unaffected due to the stable underground temperature, showing no significant temperature variations.

III. Physical Phenomena

In this section, we review the physical principles underlying the target events and conditions relevant to DAS-based manhole localization and DTS-based condition monitoring.

A. Manhole-Related Vibration Patterns from DAS Data

DAS captures vibrations along the fiber cable at 120-millisecond intervals, producing a two-dimensional array referred to as a 'waterfall.' In this 2D array, the columns correspond to spatial locations along the fiber, and the rows represent time. A colormap is used to visualize the intensity of local vibrations within this time-location plane. As such, the 2D array can be interpreted as an image. Figure 2 displays several example waterfall plots, with ground truth manhole locations indicated by the horizontal bar at the top.

Discriminative features useful for manhole localization primarily arise from vehicle interactions with the road surface and manholes, or from vibration sources inside the manhole itself. The associated vibration patterns can be categorized as follows:

- **Slack cable coils** stored in manholes or handholes are excited simultaneously when a vehicle passes by. This results in a horizontal stripe whose width corresponds to the coil length, creating two disconnected diagonal trajectories (e.g., tilted ellipse regions in Figure 2 (b)–(f)).
- **Weaker signal response** compared to neighboring cable sections, due to reduced mechanical coupling at the manhole (e.g., rounded-rectangle regions in Figure 2 (b), (d)).
- **Strong impact signatures** occur when a vehicle drives over a manhole lid, producing a significantly larger local vibration than normal driving. This interaction excites a broader section of the fiber, producing a horizontal stripe superimposed on the diagonal trajectory. (e.g., arrow-pointed regions in Figure 2 (b), (d)).
- **Vertical stripes** are caused by static or periodic vibration sources within the manhole (e.g., water pumps), which may be continuous or intermittent (e.g., rectangle regions in Figure 2 (a), (f)). Note that the vertical stripes highlighted by the hexagonal regions in Figure 2(d) are not associated with a manhole; rather, they originate from cable connections inside a large central office, where electrical appliances such as servers, power supplies, and cooling systems generate persistent vibrations.

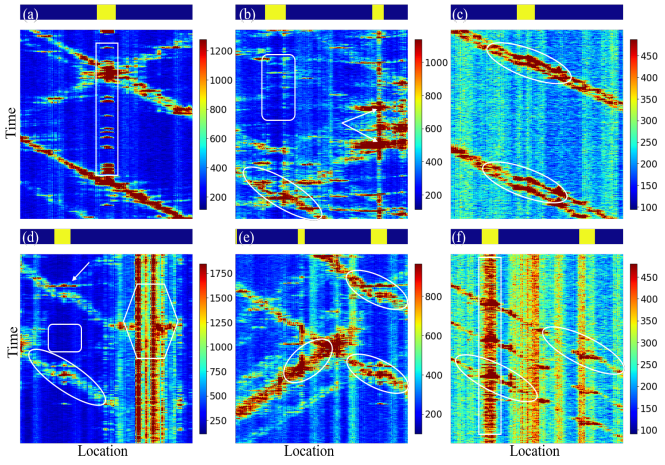

Fig. 2. Exemplary waterfall plot near manhole locations. (48-second waterfall over 418 meters; pixel color indicates vibration intensity along the cable, with warmer colors representing stronger signals (intensity reference shown by the color bar). Top bar plots: manhole locations (yellow), non-manhole locations (blue).

These phenomena enable both human analysts and machine learning models to identify manholes and slack cable loca-

tions using ambient sensing data. However, due to variability in vehicle types, driving speeds, traffic density, fiber coil lengths, and sensing distances, the resulting vibration signatures vary significantly, making rule-based detection difficult. Deep learning models [32] are well-suited for this task because they can automatically learn hierarchical and discriminative representations directly from waterfall images. By learning subtle spatiotemporal patterns and contextual cues, deep neural networks can distinguish manhole-related signals from background noise.

B. Temperature Variations from DTS Data

For manhole condition monitoring, the measured temperature variation (ΔT) played a key role. As shown in Figure 3, three different manhole (MH) and handhole (HH) conditions (dry, flooded, and iced) are illustrated in Figure 3 (a)-(c). For a dry manhole or handhole, the internal temperature during summer daytime is higher than that of the buried cable outside, while at night, it drops due to air circulation. Meanwhile, the temperature of the buried cables outside the manhole or handhole remains relatively stable, reflecting the consistent underground conditions. As a result, dry manholes or handholes exhibit a noticeable ΔT between the inside and outside across day and night cycles. In contrast, flooded and iced manholes or handholes show minimal ΔT, as the water or ice maintains a stable internal temperature throughout the day.

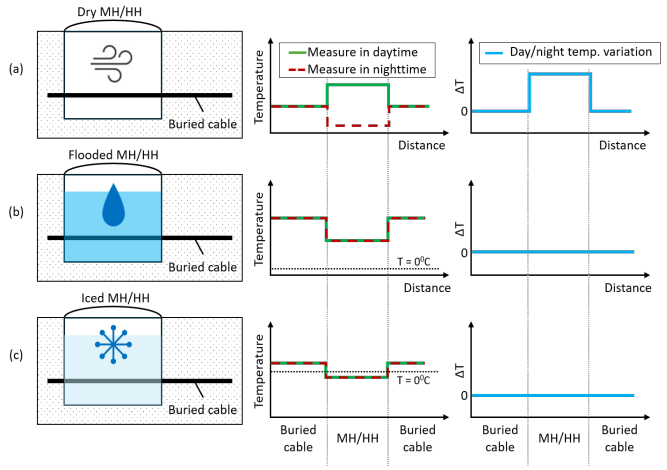

Fig. 3. Temperature variations (ΔT) in different manhole conditions

IV. Method

We explore deep learning approaches for manhole localization using ambient noise captured from DAS. With location-level labels (manhole vs. non-manhole) efficiently obtained from field survey, a machine learning model trained on DAS data from one route can be applied to localize manholes on a new route. The predictions can be cross-referenced with DTS results to further improve localization accuracy and identify flooded manholes.

A. Witness Rate Enhancement

The DAS ambient data is considered weakly labeled, as it lacks precise timestamps for events containing discriminative information. A key challenge lies in the variability of the witness rate (WR)—the frequency at which useful vibration patterns appear—across both time and location. For example, manholes are more difficult to detect during times and at locations where traffic-induced vibrations are minimal. To address this issue, we adopt a top-K data selection scheme [27], where, for each location, the K patches with the highest total vibration levels per day are selected. In our experiments, we set $K = 50$.

When the WR is high, most waterfall patches from a manhole location exhibit discriminative features—such as broken traffic trace—while only a few patches may be lack of such evidence. As a result, the problem reduces to a supervised learning task with one-sided label noise [33], that is, all negative samples (non-manhole) are truly negative. This setting can be addressed using standard supervised learning frameworks [34].

B. Structured Prediction Formulation

While manhole localization is treated as an *image classification* problem in [27], we propose a new *structured prediction*-based formulation [35] in which the labels of each column in the waterfall image are predicted as a sequence. This choice has several advantages.

1) It effectively leverages contextual information, as the label prediction is informed by neighboring locations and spatiotemporal patterns within a large window.
2) It avoids the issue of selecting an inappropriate window length, which could result in either a partial manhole or multiple manholes within the same window. This method provides fine-grained, precise label supervision at each sensing location.

To bridge the gap between different routes, we implement adaptive normalization in image preprocessing: clipping each waterfall patch at the 0.95 quantile and quantizing it into 256 levels. The waterfall image patches are resized to 256×256.

C. Model Architecture

Assuming the input image patch has a size of $H \times W$, and the output is a binary label vector of width W. When fitting a neural network model with an input of size $H \times W$ and output of size W, it is important to preserve the location (column-wise) correspondence between input and output. This inductive bias can be distilled by first auto-encoding with an intermediate representation X of size $H \times W \times C$, followed by reducing the H and C dimensions separately using an attention layer and a classifier. The architecture of the proposed **UNET-Attention** model is summarized in Table I, with the double convolution block detailed in Table II.

1) U-Net: We use a lightweight U-Net model [29] to exploit spatial-temporal dependencies in the waterfall patches, based on an encoder-decoder architecture with skip connections. The UNET-Attention architecture is detailed in Table I, with bilinear upsampling in the decoder for computational efficiency and

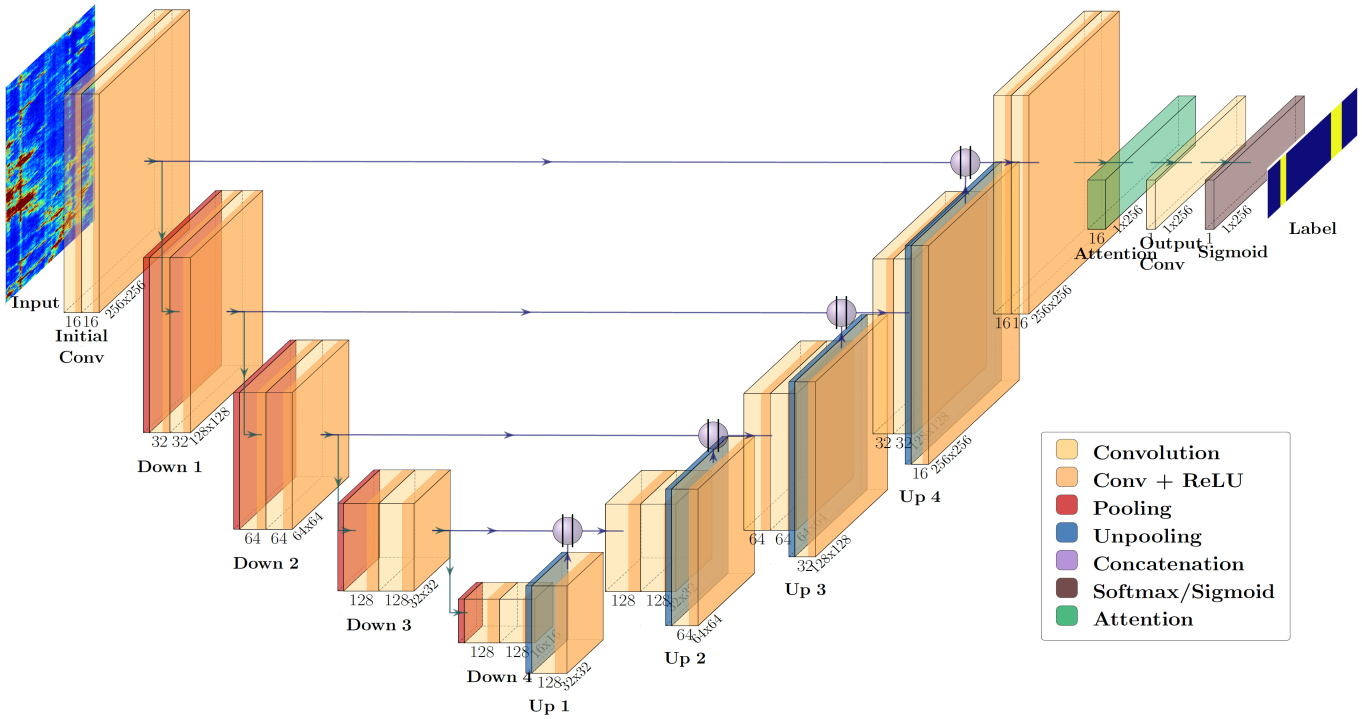

Fig. 4. Illustration of the proposed **UNET-Attention** model architecture for manhole localization formulated as a structured prediction problem. The network follows an encoder–decoder architecture with skip connections. The color-coded blocks correspond to the convolutional, pooling, unpooling, concatenation, and attention layers described in Table I. The numbers below each 3D block indicate the size of the intermediate feature maps, and arrows denote skip connections that link encoder and decoder stages [29]. The attention module enhances feature selectivity before the final sigmoid classifier, which produces dense predictions along the sensing distance dimension.

smoother feature reconstruction. The model comprises 4 down sampling blocks with increasing channels from 16 to 256, followed by 4 up sampling blocks that restore the resolution. Each downsampling block reduces the spatial and temporal resolution of waterfall images by a factor of two using stride-2 convolution, resulting in an overall downsampling factor of 16× after four stages. This hierarchical reduction allows the network to enlarge its receptive field, enabling it to integrate contextual information across both time and sensing-distance dimensions, which is crucial for distinguishing manhole-related patterns from background variations. At the same time, limiting the depth to four levels preserves sufficient spatial detail for accurate localization while keeping the model compact. The U-Net architecture has been applied to DAS to enhance spatiotemporal resolution [36] and to detect weak vehicle-induced quasi-static strain signals [37] for intelligent transportation applications.

2) Gated Attention Mechanism: We propose a time-domain attention layer to select discriminative features within the image patch along the time dimension, based on attention-based deep multiple instance learning (MIL) [27], [30]. Let $X_w = \{\mathbf{x}_{1,w}, \ldots, \mathbf{x}_{H,w}\}$ be a bag of H embeddings at location w, then the adaptive MIL pooling can be written as

$$\mathbf{z}_w = \sum_{h=1}^{H} a_{h,w}\mathbf{x}_{h,w}, \quad \mathbf{z}_w \in \mathbb{R}^C, \tag{1}$$

with a simple self-attention layer imposing soft attention pooling along the time axis H,

TABLE I
UNET-ATTENTION ARCHITECTURE OVERVIEW

Stage	Operation
Input	Input image with n_{channels}
Initial Conv	`DoubleConv`(n_{channels}, 16)
Down 1	MaxPool (×2) → `DoubleConv`(16, 32)
Down 2	MaxPool (×2) → `DoubleConv`(32, 64)
Down 3	MaxPool (×2) → `DoubleConv`(64, 128)
Down 4	MaxPool (×2) → `DoubleConv`(128, 128)
Up 1	Upsample (×2) → concat → `DoubleConv`(256, 64)
Up 2	Upsample (×2) → concat → `DoubleConv`(128, 32)
Up 3	Upsample (×2) → concat → `DoubleConv`(64, 16)
Up 4	Upsample (×2) → concat → `DoubleConv`(32, 16)
Attention	Conv1D(16,16) → Tanh → Conv1D(16,1) → Softmax
Weighted Sum	$\text{BatchedMatrixMultiplication}(\text{attn}, \text{features}^\top)$
Output Conv	1×1 Conv → Sigmoid (output n_{classes} channels)

$$a_{h,w} = \frac{\exp\left(\mathbf{w}_2^\top \tanh\left(\mathbf{W}_1 \cdot \mathbf{x}_{h,w} + \mathbf{b}_1\right) + b_2\right)}{\sum_{h'=1}^{H} \exp\left(\mathbf{w}_2^\top \tanh\left(\mathbf{W}_1 \cdot \mathbf{x}_{h',w} + \mathbf{b}_1\right) + b_2\right)}, \tag{2}$$

where the parameters $\{\mathbf{W}_1, \mathbf{w}_2, \mathbf{b}_1, b_2\}$ are dynamically predicted by a learnable network.

3) Classification:: After an out convolution layer, the final output uses a sigmoid activation to produce a $W \times 1$ probabilistic segmentation vector ($n_{\text{classes}} = 1$ for binary segmentation, Binary Cross Entropy (BCE) loss). Location-level predictions are derived by aggregating per-column predictions across multiple rows of pulse train (∼120ms) and time frames (∼48s).

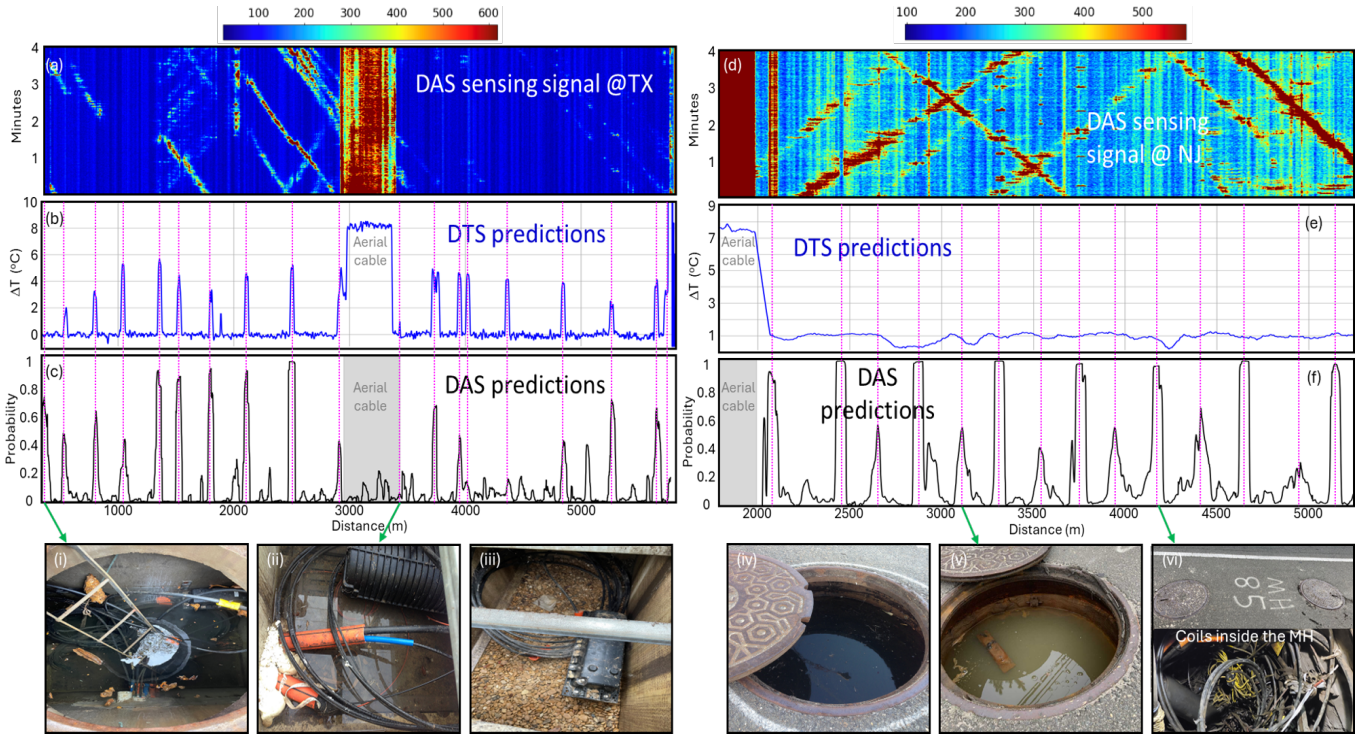

Fig. 5. Results of manhole predictions: (a–c) from Richardson, TX testbed; (d–f) from LBI, NJ testbed. (i) – (vi) photos from field manhole/handhole.

TABLE II
STRUCTURE OF THE DOUBLECONV BLOCK

Layer	Operation
1	Conv2D (in, mid) → BatchNorm2D → ReLU (in-place)
2	Conv2D (mid, out) → BatchNorm2D → ReLU (in-place)

Each `Conv2D` uses kernel size = 3, padding = 1, and no bias.

The proposed **UNET-Attention** model architecture for structured prediction (i.e., mapping a 2D image to a 1D label sequence) is illustrated in Figure 4, with the visualization generated using the PlotNeuralNet tool [38]. The encoder progressively downsamples the input waterfall image to extract multi-scale spatio–temporal features, while the decoder restores spatial resolution through bilinear upsampling and skip connections. Feature map sizes and channel dimensions are annotated below each block for clarity. The final attention block emphasizes discriminative spatial–temporal regions before classification. The number of encoder–decoder layers was empirically chosen to capture multi-scale spatio–temporal features.

V. EXPERIMENTAL RESULTS

Our method has been validated on three Verizon field testbeds in TX and NJ, demonstrating its ability to accurately localize manholes, assess conditions, and support anomaly monitoring for cable damage prevention. All experiments were conducted on a workstation running Ubuntu 22.04.5 LTS, equipped with an Intel Core i7-9800X CPU (8 cores, 16 threads, 3.8 GHz), 125 GB RAM, and one NVIDIA GeForce RTX 2080 Ti GPU (11 GB VRAM). Training for 100 epochs with a batch size of 50 takes approximately 9 hours of wall-clock time on 20,800 waterfall images (256 × 256).

A. Cross-Route Generalization

Our method demonstrates strong zero-shot cross-route generalization performance, achieving an area under the receiver operating characteristic (ROC) curve (AUC) score of 0.8463 (Richardson to LBI) and 0.8631 (LBI to Richardson) based on data collected over multiple days. With the time-domain attention layer, the AUC scores increase to 0.8766 (Richardson to LBI) and 0.8857 (LBI to Richardson). The experimental results for manhole localization predictions are presented in Figure 5, including DAS waterfall traces in (a) and (d), predictions from DTS in (b) and (e), and DAS in (c) and (f), with the actual manhole locations marked by pink lines. The test route in Richardson spans 5.8 km, with 1 km of aerial cable around 3.2 km. By setting thresholds of $\Delta T = 2°C$ and 0.45 of DAS prediction, 17 and 15 manholes were identified out of a total of 19, resulting in detection rates of 89.5% and 79%, respectively. On the Richardson route, cross-referencing DAS and DTS data improves the detection rate to 94.7%. Figure 5(i) – (iii) presents photos of manholes along the route. For the first manhole (Figure 5(i)), DTS failed to detect it as the monitoring cable was fully submerged, leading to no ΔT due to the stable water temperature. Both DAS and DTS missed another manhole (Figure 5(ii)) following the aerial cable section, attributed to short slack fibers and partial water presence inside the manhole, which reduced ΔT and resulted in low prediction probabilities from DAS.

Figure 5(iii) displays a typical dry handhole in Richardson. Using the same trained ML engines from Richardson,TX to

test the LBI, NJ route produced the result shown in Figure 5(f). This route spans 5.2 km, with an aerial cable covering the first 2 km. The DAS prediction rate was 85.7% with a threshold of 0.45. However, Figure 5(e) shows that no manholes could be detected via DTS in LBI due to the consistently flooded conditions, as evidenced in Figure 5 (iv) and (v). Figure 5(vi) shows a connected manhole with longer slack fibers, resulting in higher DAS prediction possibilities. Some manholes exhibit lower DAS prediction possibilities because they are located farther from traffic, leading to limited vibration detection. However, since ambient DAS data are abundant, incorporating additional datasets could further enhance performance. In addition, frequency-domain analysis—such as applying a fast Fourier transform (FFT) to the recorded acoustic signals—is a promising direction that could reveal additional discriminative features for identifying manhole-related events. For instance, confined spaces filled with water exhibit a filtering effect in the frequency domain, which has been evidenced experimentally utilizing DAS in [21].

B. Condition Diagnostics and Anomaly Detection

The proposed architecture is not only valuable for manhole localization but also for condition diagnostics and anomaly detection to help prevent cable damage. Figure 6(a) illustrates an enlarged DTS result of a manhole where the cable is both submerged in water and exposed to air. The corresponding field inspection is shown in Figure 6(b). By continuously monitoring these conditions, the system can provide real-time feedback to field technicians, ensuring they are equipped with the appropriate tools for maintenance, improving operational efficiency and response times.

Using the proposed scheme, we successfully identified manhole conditions under both dry and flooded scenarios. Based on the same principle, we believe that frozen manholes could also be detected, as temperature variations would similarly influence the sensing signals. However, our current field testbeds, located in Richardson, Texas, and Long Beach Island, New Jersey, did not experience freezing conditions during the testing period; therefore, we do not yet have experimental data for such cases.

Figure 6(c) and Figure 6(d) present DAS waterfall traces and DTS temperature variations for identifying cable anomalies over Philipsburg testbed (Figure 1(d)), where the fiber length is approximately 18 km. Between the 12–12.8 km section of the route (highlighted in orange), DTS detected a $\Delta T = 10^{\circ}C$, typically indicating aerial cable sections. However, DAS detected traffic patterns and behaviors that are more typical of buried cables. Cross-referencing these results suggested that the cable might have fallen from its poles or was otherwise exposed. A field inspection (Figure 6(e)) confirmed the cable had indeed fallen to the ground due to construction activities and was left unprotected. Early identification of such anomalies can help prevent potential cable damage.

VI. Conclusions

We demonstrated the effectiveness of an integrated DAS/DTS system for manhole localization, condition diagnostics, and cable status anomaly detection. By cross-referencing data from DAS and DTS, this approach significantly enhances accuracy from 79% to 94.7%, outperforming standalone systems. Field trials in Richardson, TX and Long Beach Island (LBI), NJ confirmed its adaptability to diverse environmental conditions, such as dry, and flooded manholes. Furthermore, the system's ability to provide real-time feedback to technicians ensures proactive maintenance, reducing the risk of cable damage. These results confirm that this integrated fiber sensing system is a promising solution for enhancing the operational reliability of telecom networks, particularly for 5G infrastructure and beyond.

References

[1] E. Ip, F. Ravet, H. Martins, M.-F. Huang, T. Okamoto, S. Han, C. Narisetty, J. Fang, Y.-K. Huang, M. Salemi *et al.*, "Using global existing fiber networks for environmental sensing," *Proceedings of the IEEE*, vol. 110, no. 11, pp. 1853–1888, 2022.

[2] J. Liu, S. Yuan, Y. Dong, B. Biondi, and H. Y. Noh, "TelecomTM: A fine-grained and ubiquitous traffic monitoring system using pre-existing telecommunication fiber-optic cables as sensors," *Proceedings of the ACM on Interactive, Mobile, Wearable and Ubiquitous Technologies*, vol. 7, no. 2, pp. 1–24, 2023.

[3] M. Mazur, M. Karrenbach, N. K. Fontaine, R. Ryf, V. Kamalov, L. Dallachiesa, Ö. Jonsson, A. A. Hlynsson, S. Hlynsson, H. Chen *et al.*, "Global seismic monitoring using operational subsea cable," in *ECOC 2024; 50th European Conference on Optical Communication*. Th3B7, 2024.

[4] M.-F. Huang, E. Ip, Y.-K. Huang, S. Han, J. Hu, E. Mateo, T. Wang, T. J. Xia, G. A. Wellbrock, Y. Aono *et al.*, "First field trial of hybrid fiber sensing with data transmission resulting in enhanced sensing sensitivity and spatial resolution," in *Conference on Lasers and Electro-Optics/Pacific Rim*. Optica Publishing Group, 2024, p. PDP_5.

[5] C. Wiesmeyr, C. Coronel, M. Litzenberger, H. J. Döller, H.-B. Schweiger, and G. Calbris, "Distributed acoustic sensing for vehicle speed and traffic flow estimation," in *2021 IEEE International Intelligent Transportation Systems conference (ITSC)*. IEEE, 2021, pp. 2596–2601.

[6] T. Li, Y. Chen, M.-F. Huang, S. Han, and T. Wang, "Vehicle run-off-road event automatic detection by fiber sensing technology," in *2021 Optical Fiber Communications Conference and Exhibition (OFC)*. IEEE, 2021, pp. 1–3.

[7] M.-F. Huang, S. Han, G. A. Wellbrock, T. J. Xia, C. Narisetty, M. Salemi, Y. Chen, J. M. Moore, P. N. Ji, G. Milione *et al.*, "Field trial of cable safety protection and road traffic monitoring over operational 5G transport network with fiber sensing and on-premise AI technologies," in *Optoelectronics and Communications Conference*. Optica Publishing Group, 2021, pp. T5A–8.

[8] W. S. Wilcock, S. Abadi, and B. P. Lipovsky, "Distributed acoustic sensing recordings of low-frequency whale calls and ship noise offshore central oregon," *JASA Express Letters*, vol. 3, no. 2, 2023.

[9] S. Dou, N. Lindsey, A. M. Wagner, T. M. Daley, B. Freifeld, M. Robertson, J. Peterson, C. Ulrich, E. R. Martin, and J. B. Ajo-Franklin, "Distributed acoustic sensing for seismic monitoring of the near surface: A traffic-noise interferometry case study," *Scientific Reports*, vol. 7, no. 1, p. 11620, 2017.

[10] S. Han, M.-F. Huang, T. Li, J. Fang, Z. Jiang, and T. Wang, "Deep learning-based intrusion detection and impulsive event classification for distributed acoustic sensing across telecom networks," *Journal of Lightwave Technology*, vol. 42, no. 12, pp. 4167–4176, 2024.

[11] H.-J. Li, H.-H. Zhu, D.-Y. Tan, B. Shi, and J.-H. Yin, "Detecting pipeline leakage using active distributed temperature sensing: Theoretical modeling and experimental verification," *Tunnelling and Underground Space Technology*, vol. 135, p. 105065, 2023.

[12] D. Cram, C. E. Hatch, S. Tyler, and C. Ochoa, "Use of distributed temperature sensing technology to characterize fire behavior," *Sensors*, vol. 16, no. 10, p. 1712, 2016.

[13] G. K. Ekechukwu and J. Sharma, "Well-scale demonstration of distributed pressure sensing using fiber-optic DAS and DTS," *Scientific reports*, vol. 11, no. 1, p. 12505, 2021.

[14] M. Erdmann, J. Dix, D. Ellis, G. Callender, J. Pilgrim, G. P. Lees, R. Rogers, H. R. Hansen, and T. Lucignano, "Towards active cable reburial monitoring using distributed fiber-optic sensing over 40km of a high voltage marine interconnector," in *Proc. 10th International*

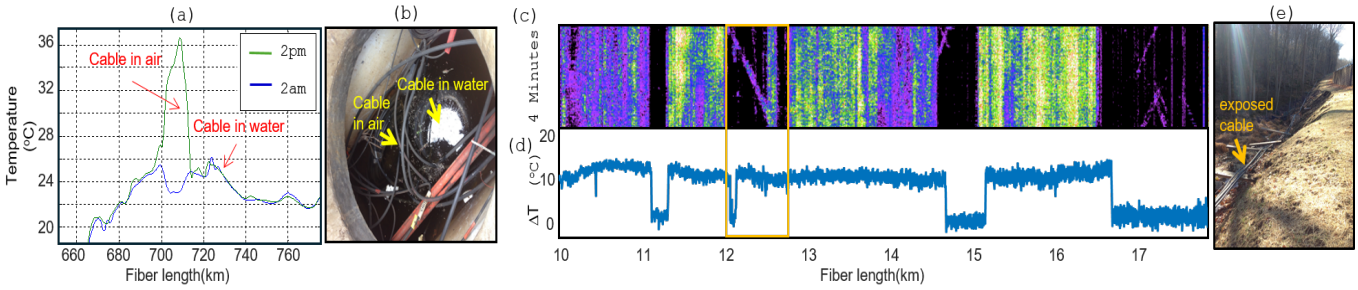

Fig. 6. Manhole condition diagnostics: (a) temperature results and (b) field inspection picture; Detected anomalies for cable damage prevention in Philipsburg, NJ: (c) DAS results, (d) DTS results and (e) field inspection picture.

Conference on Insulated Power Cables (Jicable'19), Versailles, France, 2019, pp. D9–4.

[15] V. Anand, N. Sasikumar, V. Ranjith, A. A. Ayubali, S. S. Patra, and B. Srinivasan, "Simultaneous distributed acoustic and temperature sensing for robust leakage detection in gas pipelines," in *29th International Conference on Optical Fiber Sensors*, vol. 13639. SPIE, 2025, pp. 153–156.

[16] A. Venketeswaran, N. Lalam, J. Wuenschell, P. R. Ohodnicki Jr, M. Badar, K. P. Chen, P. Lu, Y. Duan, B. Chorpening, and M. Buric, "Recent advances in machine learning for fiber optic sensor applications," *Advanced Intelligent Systems*, vol. 4, no. 1, p. 2100067, 2022.

[17] L. Shao, J. Zhang, X. Chen, D. Xu, H. Gu, Q. Mu, F. Yu, S. Liu, X. Shi, J. Sun *et al.*, "Artificial intelligence-driven distributed acoustic sensing technology and engineering application," *PhotoniX*, vol. 6, no. 1, p. 4, 2025.

[18] S. Lapins, A. Butcher, J.-M. Kendall, T. S. Hudson, A. L. Stork, M. J. Werner, J. Gunning, and A. M. Brisbourne, "DAS-N2N: machine learning distributed acoustic sensing (DAS) signal denoising without clean data," *Geophysical Journal International*, vol. 236, no. 2, pp. 1026–1041, 2024.

[19] Z. Jiang, Y. Tian, Y. Ding, S. Ozharzr, and T. Wang, "DiffOptics: A conditional diffusion model for fiber optics sensing data imputation," in *2025 Optical Fiber Communications Conference and Exhibition (OFC)*. IEEE, 2025, pp. 1–3.

[20] H. Wang, X. Yang, S. Zeng, T. Liu, X. Wang, and Y. Wang, "Deep learning model for fiber optic distributed acoustic sensing seismic data compression based on autoencoder and recurrent neural networks," *Applied Optics*, vol. 63, no. 20, pp. 5303–5315, 2024.

[21] J. M. Marin, W. H. Gunawan, A. Rjeb, I. Ashry, B. Sun, T. Ariff, C. H. Kang, T. K. Ng, S. Park, C. M. Duarte *et al.*, "Marine soundscape monitoring enabled by artificial intelligence-aided integrated distributed sensing and communications," *Advanced Devices & Instrumentation*, vol. 6, p. 0089, 2025.

[22] J. Sun, S. Han, W. Kohno, and C. Chen, "CLAP-S: Support set based adaptation for downstream fiber-optic acoustic recognition," in *ICASSP 2025-2025 IEEE International Conference on Acoustics, Speech and Signal Processing (ICASSP)*. IEEE, 2025, pp. 1–5.

[23] S. Han, M.-F. Huang, T. Li, S. Kotrla, J. A. Mundt, T. Wang, and Y. Aono, "Energy-based generative models for distributed acoustic sensing event classification in telecom networks," in *Proceedings of the 51st European Conference on Optical Communication (ECOC 2025)*, Copenhagen, Denmark, Sep. 2025.

[24] G. A. Wellbrock, T. J. Xia, M.-F. Huang, S. Han, Y. Chen, T. Wang, and Y. Aono, "Explore benefits of distributed fiber optic sensing for optical network service providers," *Journal of Lightwave Technology*, vol. 41, no. 12, pp. 3758–3766, 2023.

[25] M. Wada, Y. Maeda, H. Shimabara, and T. Aihara, "Manhole locating technique using distributed vibration sensing and machine learning," in *Optical Fiber Communication Conference*. Optica Publishing Group, 2021, pp. Tu1G–3.

[26] Y. Lu, Y. Tian, S. Han, E. Cosatto, S. Ozharar, and Y. Ding, "Automatic fine-grained localization of utility pole landmarks on distributed acoustic sensing traces based on bilinear resnets," in *ICASSP 2021-2021 IEEE International Conference on Acoustics, Speech and Signal Processing (ICASSP)*. IEEE, 2021, pp. 4675–4679.

[27] A. Bukharin, S. Han, Y. Chen, M.-F. Huang, Y.-K. Huang, Y. Xie, and T. Wang, "Ambient noise-based weakly supervised manhole localization methods over deployed fiber networks," *Optics Express*, vol. 31, no. 6, pp. 9591–9607, 2023.

[28] M.-F. Huang, S. Han, Y. Li, G. A. Wellbrock, T. J. Xia, S. Kotria, J. M. Moore, P. Ji, T. Li, Y. Chen *et al.*, "Field trials of manhole localization and condition diagnostics by using ambient noise and temperature data with AI in a real-time integrated fiber sensing system," in *Optical Fiber Communication Conference*. Optica Publishing Group, 2025, p. M1C1.

[29] O. Ronneberger, P. Fischer, and T. Brox, "U-net: Convolutional networks for biomedical image segmentation," in *Medical Image Computing and Computer-Assisted Intervention–MICCAI 2015: 18th International Conference, Munich, Germany, October 5-9, 2015, proceedings, part III 18*. Springer, 2015, pp. 234–241.

[30] M. Ilse, J. Tomczak, and M. Welling, "Attention-based deep multiple instance learning," in *International Conference on Machine Learning (ICML)*. PMLR, 2018, pp. 2127–2136.

[31] E. Ip, J. Fang, Y. Li, Q. Wang, M.-F. Huang, M. Salemi, and Y.-K. Huang, "Distributed fiber sensor network using telecom cables as sensing media: technology advancements and applications," *Journal of optical communications and networking*, vol. 14, no. 1, pp. A61–A68, 2022.

[32] Y. Bengio, A. Courville, and P. Vincent, "Representation learning: A review and new perspectives," *IEEE Transactions on Pattern Analysis and Machine Intelligence*, vol. 35, no. 8, pp. 1798–1828, 2013.

[33] A. Blum and A. Kalai, "A note on learning from multiple-instance examples," *Machine learning*, vol. 30, pp. 23–29, 1998.

[34] M.-A. Carbonneau, V. Cheplygina, E. Granger, and G. Gagnon, "Multiple instance learning: A survey of problem characteristics and applications," *Pattern Recognition*, vol. 77, pp. 329–353, 2018.

[35] J. Lafferty, A. McCallum, F. Pereira *et al.*, "Conditional random fields: Probabilistic models for segmenting and labeling sequence data," in *International Conference on Machine Learning (ICML)*, vol. 1, no. 2. Williamstown, MA, 2001, p. 3.

[36] S. Yuan, M. van Den Ende, J. Liu, H. Y. Noh, R. Clapp, C. Richard, and B. Biondi, "Spatial deep deconvolution u-net for traffic analyses with distributed acoustic sensing," *IEEE Transactions on Intelligent Transportation Systems*, vol. 25, no. 2, pp. 1913–1924, 2023.

[37] F. Peng, Z. Zhu, Y. Zhang, and Q. Miao, "A deep learning image segmentation model for detection of weak vehicle-generated quasi-static strain in distributed acoustic sensing," *IEEE Transactions on Intelligent Transportation Systems*, 2025.

[38] H. Iqbal, "PlotNeuralNet: Latex code for drawing neural networks," 2018. [Online]. Available: https://doi.org/10.5281/zenodo.2526395